Research Article Vol. 12, No. 9 / 1 Sep 2022 / Optical Materials Express 3493
Optical Materials EXPRESS

Rare-earth doped transparent oxyfluoride glass-ceramics: processing is the key [Invited]

María Eugenia Cruz,[1] Mercedes Sedano,[1] Yolanda Castro,[1] María Jesús Pascual,[1,*] Joaquín Fernández,[2] Rolindes Balda,[3,4] and Alicia Durán[1]

[1]Instituto de Cerámica y Vidrio (CSIC), Campus de Cantoblanco, 28049 Madrid, Spain
[2]Donostia Internacional Physics Center (DIPC), 20018 San Sebastian, Spain
[3]Dept. Física Aplicada, Escuela Superior de Ingeniería, Universidad del País Vasco (UPV-EHU), 48013 Bilbao, Spain
[4]Centro de Física de Materiales (UPV/EHU-CSIC), 20018 San Sebastian, Spain
*mpascual@icv.csic.es

Abstract: Oxyfluoride glass-ceramics (OxGCs) are transparent materials composed by an oxide glass matrix with homogeneously distributed fluoride nanocrystals. In particular, OxGCs with RE-doped lanthanide-fluoride nanocrystals are of special interest for photonic applications. More than 600 publications including several review papers were indexed on Scopus related to "glass-ceramics" revealing the importance of the topic. Melt-quenching followed by thermal treatment, is the most used preparation method, which allows materials in bulk and fibre form to be obtained, being also a scalable industrial process. Spark plasma sintering from glass powders is showing promising results. The sol-gel process has appeared as an alternative method to avoid some of the drawbacks of the melting process such as the high temperature. It also permits to process materials with different shapes such as thin films, nano-sized powders or bulk materials at very low temperature. This paper reviews the different aspects involved in the preparation of OxGC materials by melt-quenching, spark plasma sintering and sol-gel and how the processing parameters directly affect the glass-ceramics properties from results of the GlaSS research group from CSIC. A comparison of the thermal, structural and optical properties is discussed along with some perspectives for preparing other advanced materials within this field.

1. Introduction

Glass-ceramics (GCs) are inorganic non-metallic materials prepared by controlled crystallization of glasses via different processing methods. GCs contain at least one type of functional crystalline phase precipitated in a glass matrix. The volume fraction crystallized may vary from ppm to almost 100% [1]. In particular, fluoride phases are good hosts to be doped with Rare-earth (RE) ions, reducing the probabilities of multiphonon relaxation, thus resulting in longer lifetimes of the excited state, and higher luminescence efficiencies [2,3]. Oxyfluoride glass-ceramics (OxGCs), with lanthanide fluoride crystals embedded, have demonstrated significant improvement of the optical properties of oxide glasses since the nineties. Since Wang Y. and Ohwaki J. [4] pioneer work, these materials have gained more interest and started to be intensely studied, with relevant papers published in the last years [5–7]. The excellent mechanical, thermal and chemical properties of the oxide glass matrix are combined with the low maximum phonon energy, optical transparency and rare-earth ions solubility of fluoride nanocrystals. Lanthanide-fluoride nanocrystals show very low phonon energy (250-450 cm^{-1}) in comparison to the phosphate or silicate glasses (around 1200 cm^{-1} and 1100 cm^{-1}, respectively). OxGCs applied in photonics must be transparent, avoiding the scattering produced by the different refractive index between the NCs and the glass matrix. To achieve this effect, NCs sizes must be under nanometer range (less than 50 nm). Traditionally, oxyfluoride glass-ceramics have been prepared using

#462684 https://doi.org/10.1364/OME.462684
Journal © 2022 Received 29 Apr 2022; revised 17 Jun 2022; accepted 20 Jun 2022; published 10 Aug 2022

Optical Materials EXPRESS

the melt-quenching (MQ) method where the raw materials are melted at high temperatures (1400–1700 °C) for obtaining the parent glass. The glass composition must be carefully designed to generate the precipitation of the desired fluoride crystal phases during the thermal treatment.

During the MQ, the crystallization process of the parent glass is performed at temperatures slightly higher than the glass transition temperature (T_g, $T_g \pm 20$–100 °C) for long times (from 3 h to 120 h) [5,8–10]. For example, in the case of LaF_3 GCs, the crystallization occurs via droplets of La and Si-phase separation in the parent glass followed by controlled cooling to room temperature. During this process, a diffusion-controlled mechanism is considered and a silica barrier is formed around the crystals limiting the crystal growth [11–14]. Many OxGC compositions have been designed and prepared, demonstrating enhanced optical properties compared to corresponding glasses [15,16]. Nowadays, MQ is the most used production process for OxGCs, being an industrially scalable method. Different fluoride phases such as LaF_3, $NaGdF_4$, $NaLaF_4$ or $KLaF_4$ [17–22] have been successfully obtained by MQ and more recently, optical fibres with OxGCs core have been also prepared, being a very promising goal [23–25].

Although, MQ has numerous advantages, some drawbacks are identified. The high melting temperatures cause important fluorine loss (around 30- 40 mol%.) affecting the final composition and making impossible to control the amount of fluorine and lanthanides ions in the final material. In addition, an initial amount of fluoride too high can provoke premature crystallization leading to compositional inhomogeneity and an opaque final GC [26]. The result is a strong limitation of the percentage of active phase that can be incorporated. Regarding the RE incorporation, different studies demonstrate that part of the RE ions remain in the glass matrix, not entering in the fluoride nanocrystals, due to the high viscosity that limits the ionic diffusion, thus reducing the optical efficiency of the OxGCs [27]. Another important shortcoming of MQ is the preparation of thin films, not possible by this method.

Alternative processes have been proposed in the last decades looking for preparing OxGCs with higher fluoride contents and increased contents of RE-ions incorporated into the NCs. Spark Plasma Sintering (SPS) is an attractive method to prepare transparent GCs [28–30]. This method allows transparent materials in short times to be obtained, compared to the conventionalthermal treatment in a furnace, that usually takes long times (10-100 hours). Riello et al. [31] published in 2006 the first work on Li_2O- Al_2O_3- SiO_2 (LAS) GCs doped with erbium and obtained by SPS. Different glass-ceramics compositions, such as chalcogenides or oxyfluorides, have been prepared by this method. Chalcogenide transparent tellurite glasses and GCs were prepared in 2013 by Betrand et al. [32]; however, carbon contamination is still a drawback for optical applications. Currently, there are not many papers about OxGCs processed by SPS. Recently, different oxyfluoride crystalline phases have been obtained by the GlaSS group of the Institute of Ceramics and Glass (CSIC) such as $KLaF_4$ [33], $NaLaF_4$ and $NaLuF_4$, these two last ones not published yet. For these OxGCs the precursor glasses were prepared by melting and after grinding and sieving the glass powders were used for SPS sintering.

On the other hand, Sol-Gel (SG) is a flexible and low-temperature method, established as a promising route for the preparation of OxGCs in the nineties. Fujihara et al. [34] reported for the first time sol-gel OxGCs based in LaF_3 nanocrystals precipitated in a silica matrix. Fuhijara's method, called "TFA route", consists on the preparation of two sols, one to form the silicate matrix, starting from metal alkoxides, and the second prepared by mixing acetates, nitrates, or chlorates of the correspondent Ln^{3+} dissolved in a fluorine acid, commonly trifluoroacetic acid (TFA) as precursor of the LnF_3 or $LnRF_4$ nanocrystals. Finally, the two sols are mixed in suitable proportions to get the desired composition. Fluoride nanocrystals crystallize during a controlled heat-treatment of the silicate xerogel at low temperature and varying the sintering time between 1 min and 20 hours. To achieve the fluoride crystallization a reaction between TFA and the lanthanides acetate occurs (Eq. 1) [35]. TFA ions surround the Ln^{3+} ensuring the further

Optical Materials EXPRESS

precipitation with fluorides:

$$La(CF_3COO)_3 \rightarrow LaF_3 + (CF_3CO)_2O + CO + CO_2 \qquad (36) \qquad (1)$$

Fujihara et al. [35] explained that when the active phase is higher than 15 wt.%, the resulting OxGCs are not transparent due to a simultaneous undesired crystallization of LaOF with LaF_3. Several compositions have been prepared following this route without any synthesis modification, including single phases such as CaF_2, BaF_2, SrF_2, or more complex ones like $BaMgF_4$ [36–39]. In all cases, the active phase was between 5-10 wt. % and final composition was not measured neither estimated.

More recently, Gorni et al. [40] modified the synthesis route proposed by Fujihara and the crystallization treatment, strongly reducing the treatment time from 20 h to 1 min. The studies carried out by the GlaSS group served to establish the crystallization mechanism of sol-gel OxGC materials, and also reported obtaining OxGCs in the LaF_3-SiO_2 system with active phase of 18 wt.% calculated by Rietveld refinement, the higher published up to our knowledge. Other phases were also prepared by GlaSS group following similar procedures, such as $NaGdF_4$, $NaLaF_4$, and $KLaF_4$ [8,40,41].

On the other hand, a few papers have reported OxGCs thin films prepared by sol-gel following Fujihara's route, but without conclusive optical results [35]. Due to the rapid densification of the films, crystal are too small (around 2.5 nm), generating very low luminescence emissions.

In the last years, GlaSS group has proposed an alternative sol-gel route, called "Pre-crystallized nanoparticles route", based in the incorporation of fluoride nanocrystal suspensions into a silica sol to ensure a suitable morphology and size of the fluoride NCs and achieve the desire properties of thin films.

The aim of this work is to compare materials with similar fluoride phases prepared by different processing methods, MQ, SPS and SG. A brief state of the art of OxGCs processing routes with different crystal phases is presented, focusing in highlighting the advantages and drawbacks of each technique and the materials that can be obtained in each case. Thus, it will be possible to decide the most suitable process for each shape and application.

2. Processing routes

The most relevant details of the different synthesis routes for the analysed processes above are described in the following:

2.1. Melt-quenching (MQ)

Melt-quenching is the most traditional technique to make glass and includes the mix of different reagents of a selected composition (mol%) and then heating in an electric furnaces for melting. In general, the batches were calcined and then melted in air atmosphere at temperatures between 1450 to 1700 °C depending on the composition, being after poured onto brass moulds [14,42–45]. Some authors [21,46–49] use a second melting to improve the homogeneity. The glasses were further annealed to eliminate stresses. The corresponding GCs are obtained after thermal treatment of the parent glasses at temperatures slightly higher than the glass transition temperature (T_g + 20-100 °C) during different times (between 3 to 120 h) [10,50].

2.2. Spark plasma sintering (SPS)

There are different methodologies for producing GCs by SPS. All start from preparing the glass powders with suitable particle size by milling and sieving the precursor glass produced by MQ or sol-gel method [28,30,31,51]. Then, the glass powder can be pre-compacted to obtain a pellet [32,52,53] that it is pre-heat treated at temperatures below to T_g [28,32,33] or directly sintered in the SPS equipment [29,54–57]. In both cases, samples are sintered in vacuum conditions though

Optical Materials EXPRESS

the generation of spark plasma with the simultaneous application of pressure, temperature and pulsed direct current (ON/OFF). SPS process is controlled by changing three main parameters: maximum pressure, dwell temperature and holding time, although the particle size of the glass powder is also a determining parameter to obtain transparent final GC materials [28,33,58].

This method is suitable for obtaining well-densified and highly homogeneous glass-ceramics in relatively short times, but it presents a serious drawback related with the carbon contamination coming from the used die and graphite pistons. Different authors [28,29,33,59] have tried to reduce or even eliminate this contamination using protective foils of molybdenum, alumina, platinum or tantalum and/or applying a pre-sintering treatment.

2.3. Sol-gel process

The sol-gel process is an alternative low-temperature approach to obtain GCs materials avoiding the drawback of MQ. Several steps are involved in the SG synthesis beginning, in most cases, with the mixing of metal alkoxides and their corresponding hydrolysis. The following steps depend on the sol-gel route.

2.3.1. TFA route

LaF_3-OxGCs doped with Nd^{3+} self-supported layers are obtained from tetraethylorthosilicate (TEOS), acidic water (H_2O, 0.1 M HCl), ethanol (EtOH), trifluoroacetic acid (TFA) and lanthanum acetate ($La(CH3COO)_3$), Nd^{3+} being added as acetate. The SiO_2 sol is prepared using a molar ratio 1TEOS:2H_2O (0.1 HCl):9.5EtOH and stirring for 2 h at room temperature. Separately, 1$La(CH_3COO)_3$:5EtOH:5TFA:4H_2O with $Nd(CH_3COO)_3$ is mixed and stirred for 2 h at 40 °C. Nd^{3+} doped-80SiO_2-20LaF_3 composition was obtained by mixing the corresponding volumes of SiO_2 sol with the La solution [27].

$KLaF_4$-OxGCs was also prepared following a similar process of LaF_3-OxGCs. First, 1$La(CH_3COO)_3$:0.95K(CH_3COO):5EtOH:5TFA:4H_2O and 0.1 mol% of Nd^{3+} as acetate were mixed and stirred for 2 h at 40 °C. Separately, a SiO_2-sol was obtained by mixing 1TEOS:2H_2O (0.1M HCl):3.5EtOH and stirred for 2 h at room temperature. Finally, 80SiO_2-20$KLaF_4$ sol was obtained from mixing the corresponding amounts of silica sol and La-solution. The as-prepared sol was first dried and then further heat-treated between 350 °C and 650 °C for different times in order to reach LaF_3 crystallization.

2.3.2. Pre-crystallized nanoparticles route

The suspensions of Nd^{3+}-doped LaF_3 nanoparticles were prepared using lanthanum chloride ($LaCl_3$), ammonium fluoride (NH_4F) and neodymium acetate ($Nd(CH_3COO)_3$) as reagents in a molar ratio 1$LaCl_3$:1NH_4F:0.009$Nd(CH_3COO)_3$ and deionized water to reach a La^{3+} concentration of 0.04 M. The suspension was maintained at 75 °C for 2 h in continuous stirring. Then, polivinylpirrolidone (PVP) was added as dispersant to the solution in a relationship 10 wt% of PVP respect to LaF_3 content. Subsequently, the suspension was concentrated using a rotary evaporator (R-210 with vacuum pump V-700, Buchi) to reach a final concentration of 0.25 M.

To obtain the Nd^{3+} doped-20LaF_3–80SiO_2 sols, 14.5 ml of tetraethyl orthosilicate (TEOS, Sigma Aldrich) and 13 ml of methyl-triethoxysilane (MTES, ABCR) were mixed and incorporated to the corresponding amount of Nd^{3+} doped LaF_3 suspension. Then, HCl was directly added under continuous stirring to reach an homogenous sol.

3. Comparative study of OxGCs containing LaF_3 prepared by MQ and SG

OxGCs containing LaF_3 have been studied since the nineties due to their high RE solubility, low phonon energy, and good thermal and environmental stability. Moreover, this fluoride is quite suitable for hosting rare earth ions (RE), since La^{3+} has a similar ionic radius and valence

Optical Materials EXPRESS

than other lanthanides used as dopants [60]. These properties convert LaF_3 in a very attractive fluoride for highly efficient glass-ceramics in optics. LaF_3 is present in cubic (α) and hexagonal (β) phases, the last being more stable [15]. In the last decades, many advances were published on LaF_3-OxGCs, with promising results. In this section, LaF_3-OxCGs processing by MQ and SG methods are compared, including the characterisation of products and efficiency of optical behaviour.

3.1. Structural characterization

Dejneka [15] in 1998 prepared Eu^{3+}-doped transparent LaF_3 OxGCs by MQ with good optical results. The authors have described the growth of LaF_3 in an aluminosilicate glass that occurs by annealing above the glass transition temperature (650°C). A first phase separation appears with droplets enriched on La-Si; during the heat treatment; crystallization process proceeds with multiple LaF_3 crystallites growing inside each droplet. The authors have demonstrated that the luminescence emission spectra of a Eu^{3+}-doped LaF_3- alumosilicate system turn more defined for higher heat-treatment temperatures (around 675°C).

After the improvements revealed by Dejneka [15], T. Xu, Y. et al. [61] studied a composition with less silica $40SiO_2$-$30Al_2O_3$-$18Na_2O$-$12LaF_3$ doped with 0.5-1% Pr/YbF_3 by differential thermal analysis (DTA). They assigned a crystallization peak around 610°C, this temperature depending on the dopant amount, that affects the glass viscosity.

De Pablos-Martin et al. [17] and Gorni et al. [48], from GlaSS group, described the crystallization kinetics of LaF_3-OxGCs with composition $55SiO_2$–$20Al_2O_3$–$15Na_2O$–$10LaF_3$ (55Si10La) doped with 0.1–2 mol% NdF_3. Figure 1(a) shows the differential thermal analysis (DTA) at different heating rates for the base glasses. The exothermic peak in the range of 650 °C-750 °C is assigned to the crystallization of LaF_3, being present from the heating rate of 10 °C/min. It was also observed a linear relation between glass transition temperature (T_g) and concentration of dopant (black points in Fig. 1(b)) starting from 575 °C for 0.1%NdF_3-55Si10La up to 590 °C for a 2%NdF_3-55Si10La, while the crystallization temperature (T_p) remains almost stable (around 675 °C). The result of the evolution of T_g and T_p implicates a reduction of the crystallization stability parameter ($\Delta t = T_p$-T_g) and a higher tendency to crystallization. The effect of the dopant agrees with that reported by Chen, D. et al. [62], who argued that RE dopants act as nucleating agents, favouring phase separation and increasing the viscosity of the glass.

Figure 2(a) shows a DTA/TG analysis for 0.1Nd^{3+}-doped 55Si10La system obtained by MQ. The crystallization peak (1) appears around 750 °C and the losses detected by thermogravimetric analysis (TG) are attributed to residual fluorine losses in the amorphous matrix during the heat-treatment. Gorni et al. [63] confirmed the presence of LaF_3 as unique phase by X-Ray diffraction (XRD) for 55Si10La (Fig. 3(a)), revealing an increment of the peaks intensity up to 5 h of treatment and a further stabilization. This was also confirmed by the crystal size calculation, with growth increasing during the first hours of treatment, further maintaining around 11 nm, Fig. 3(c). Moreover, the authors reported that the crystal size decreases gradually when the concentration of Nd^{3+} increases due to the higher density, involving a higher T_g, that delays the crystallisation mechanism. Rietveld refinement calculation showed that crystal fraction varies with changing the dopant content. A clear increase of crystalline fraction is appreciated above 0.5 mol% NdF_3 (9.9 wt%) and, a stabilization or a slightly decrease of the crystal fraction (8.8 and 8.2 wt% crystalline fraction) is observed at higher concentrations of dopant (1 and 2 mol%).

Gorni et al. [48] confirmed the distribution of crystal size by HR-TEM revealing droplets with medium size of 34.0 ± 0.4 nm (Fig. 4(a) and 4(d)); after a heat-treatment of 40 h at 620 °C, LaF_3 crystals of around 12 nm appear inside the droplets. The presence of the crystal planes [111] and [113] corresponding with the d-space 0.33 nm (2θ= 27.5°) and 0.20 nm (2θ= 44.7°), respectively, confirm the presence of LaF_3 crystalline phase (JCPDS 00 032 0483). Figure 4 b shows the EDX analysis performed for two adjacent nanoparticles (Fig. 4 c) with a red circle.

Optical Materials EXPRESS

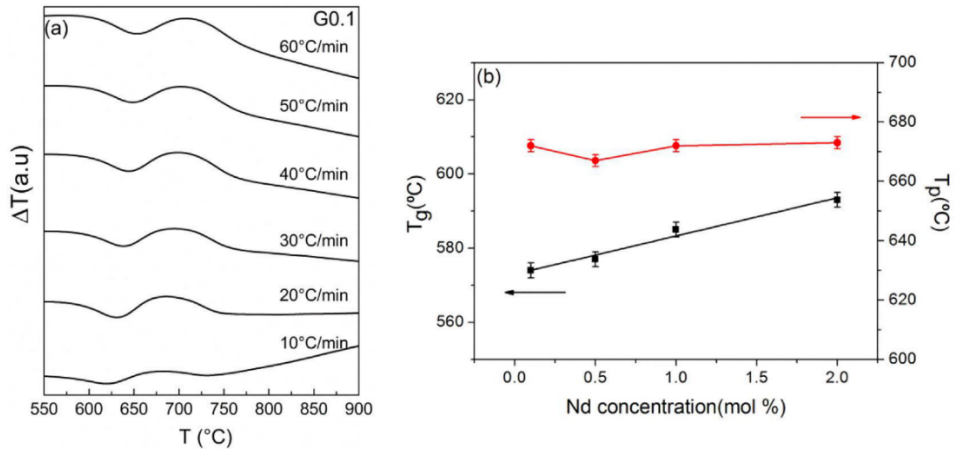

Fig. 1. (a) DTA curves at different heating rates of the $0.1Nd^{3+}$-55Si10La glass prepared by MQ and (b) T_g variation with Nd^{3+} concentration of the 55Si10La prepared by MQ with heating rate of 10°C/min, (black points represents the T_g values and red points the T_p ones). *Adapted from* [48], *copyright (2017), with permission from Elsevier*.

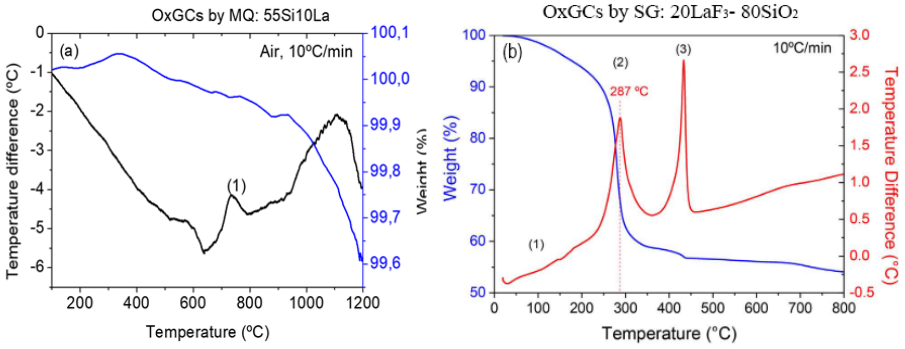

Fig. 2. DTA and TG results performed in air using a rate of 10 °C/ min for (a) 55Si10La prepared by MQ at 1650 °C. The exothermic peak (a) of the DTA is associated to the LaF_3 crystallization, while the mass loss in the TG is attributed to fluorine losses. (b) $20LaF_3$-$80SiO_2$ prepared by SG. The endothermic peak (1) is assigned to solvent removal. The exothermic peaks (2) and (3) as associated to LaF_3 crystallization and combustion process, respectively. *Adapted from* [40], *copyright (2018)*.

Optical Materials EXPRESS

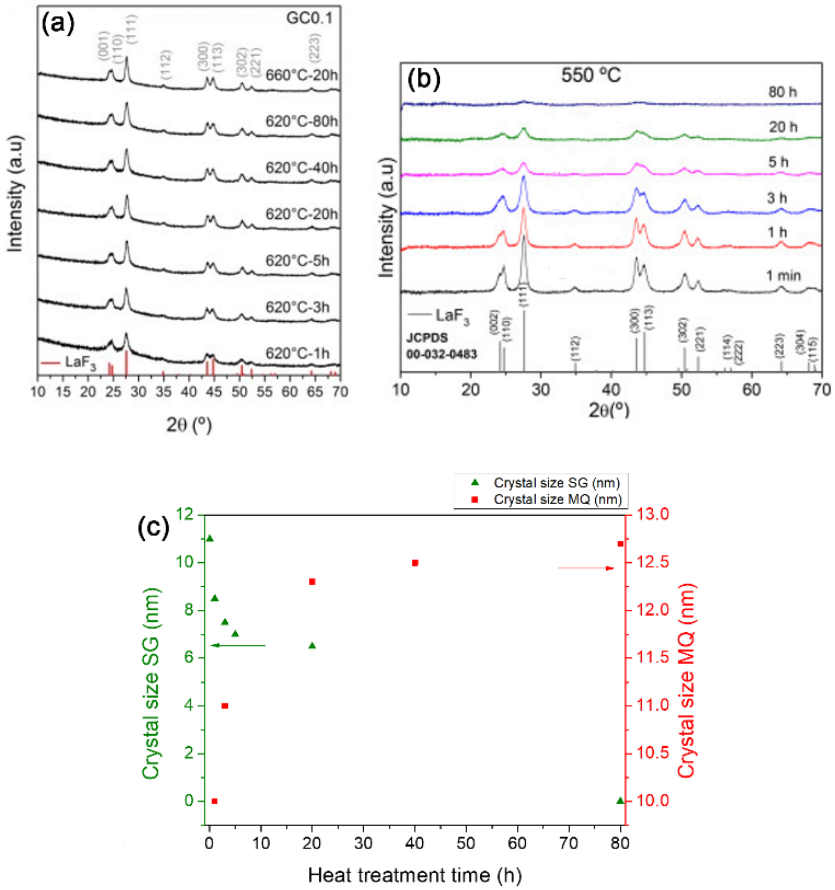

Fig. 3. (a) XRD of 55Si10La GCs prepared by MQ at different treatment times (0-80 h) presenting LaF_3 crystallisation for all times. *Adapted to* [48], *copyright (2017), with permission form Elsevier.* (b) XRD of $80SiO_2$-$20LaF_3$ sol-gel glass-ceramics treated at 550 °C from (0-80 h). *Adapted from* [40], *copyright (2018)* (c) Crystal size evolution for GCs prepared by MQ (55Si10La) and SG ($20LaF_3$-$80SiO_2$).

Optical Materials EXPRESS

The points 1-2 and 3-4 delimit both nanoparticles, and yellow line indicated the scanning line. EDX analysis of Fig. 4(b) shows a Si enrichment surrounded around the nanoparticles, which hinders further crystal growth.

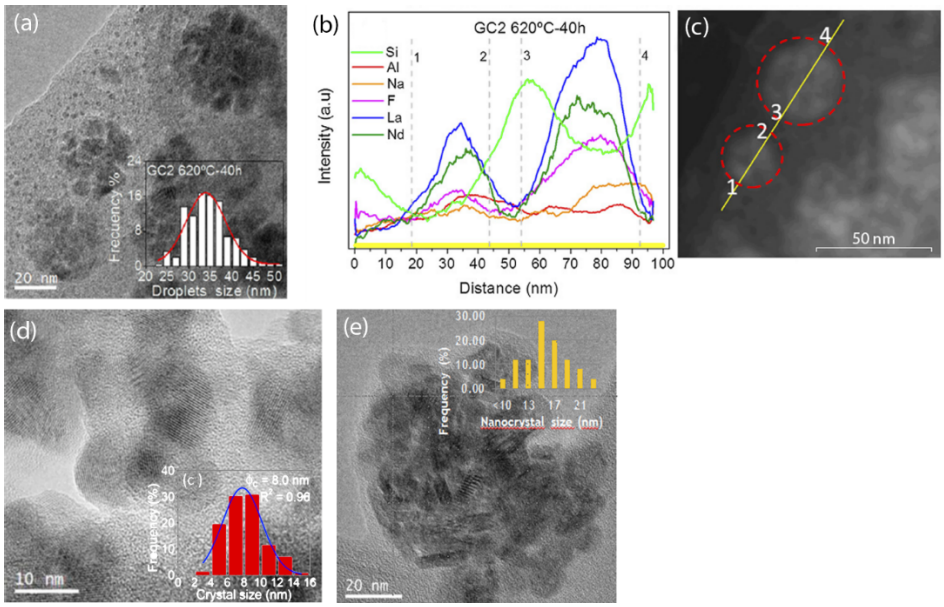

Fig. 4. HR-TEM images taken from (a) 55Si10La GCs prepared by MQ after a heat treatment of 40h at 620 °C and its corresponding crystal size distribution, with a medium size around 35 nm. (b) EDX of 55Si10La showing along two droplets containing several crystals. (c) STEM image of the droplets presented in "b" in the EDX measurement where the yellow line represent the scanning. *Adapted fom* [48], *copyright (2017), with permission from Elsevier*. (d) $20LaF_3$-$80SiO_2$ GC prepared by SG (classical route) heat-treated at 550 °C for 1min and the corresponding crystal size distribution with a medium size of 8nm. (e) $20LaF_3$-$80SiO_2$ GC prepared by SG (new route) and its corresponding crystal size distribution with a medium size of 16 nm. *Adapted from* [67], *copyright (2020)*.

Gorni et al. [64] have also prepared OxGCs fibres from MQ glasses with composition 55Si10La by single crucible method. The glass fibre was covered with a multilayer sol-gel coating deposited by dip-coating and annealed at 450 °C/ 1 h to densify the SiO_2 film. XRD results of bulk and fibres samples permitted to identify a delay in the crystallization kinetics of the fibres that needed much higher heat-treatment time (120 h) to achieve LaF_3 crystals at 620 °C, this behaviour being explained by the higher cooling rate of the drawing process. Crystals of 14-15 nm medium size appears in fibres with similar shape of those obtained for bulk.

Although, the MQ results are very interesting, the main drawbacks of this process are associated with the limitation of the crystal fraction that can be incorporated, along with the high temperatures required. Sol-gel process appeared as a promising technique to solve these problems.

Our group [40] have studied the crystallization mechanism of Er^{3+}-doped LaF_3-SiO_2 system from a precursor xerogel.

Figure 2(b) shows the DTA analysis performed at 10 °C/ min in air atmosphere (Fig. 2 b) for the OxGCs obtained by SG, together with the TG curve. Two weight losses are identified, the first one corresponding to the solvent elimination. A big mass loss appears in the thermogravimetric curve (TG) between 250 °C to 380 °C, indicating that the chemical reaction described in the Eq. (1) took place together with the crystallization. In agreement with the TG curve, the first exothermic peak (2) represented in the DTA curve is related to the crystallization of fluoride crystals. The second

Optical Materials EXPRESS

exothermic peak (3) (around 450 °C) is associated with the combustion process (Fig. 2 b). The different behaviour observed in the DTA and TG for MQ and SG (Fig. 2), reveals two different crystallization processes. For 55Si10La (MQ), a less intense peak accompanied with a slow mass decrease is observed while in the SG sample a very clear and intense peak is observed, indicating that the precipitation and a chemical reaction occur simultaneously. Many authors studied the crystallization of LaF_3 in sol-gel oxyfluoride glass-ceramics using long heat-treatments or high temperatures (700 °C-1000 °C) and observing the precipitation of small LaF_3 crystals together with other co-precipitated phases. [65] For example, the crystallization of the LaOF along with LaF_3 takes place at temperatures higher than 600 °C. [66]

A significant processing change was introduced by Gorni et al. [40] in 2018, reporting that no high temperature neither long sintering times are necessary to get suitable crystallization of LaF_3 OxGCs. The crystallization of LaF_3–SiO_2 system was followed by DRX showing that increasing temperature treatments lead to a re-dilution of fluorides in the matrix. Figure 3(b) shows intense peaks of LaF_3 achieved when samples are sintered at 550 °C for 1 min, while for longer heating times, up to 80 h, no crystals are present. This study also permited to identify bigger crystals for a one-minute heat-treatment with sizes decreasing when treatment time increases. Figure 3(c) shows the decrease of crystal size for $20LaF_3$-$80SiO_2$ sol-gel system as a function of time treatment.

The different behaviour observed by DTA/TG and DRX in OxGC produced by MQ and SG confirms that the crystallization mechanism is totally different. A diffusion-controlled process with a nucleation step and a further growing of the crystals occurs in MQ, whereas in sol-gel materials the crystallization process occurs through a chemical reaction that takes place simultaneous precipitation of crystals. [40]

Gorni et al. [27] have calculated by Rietveld refinement the real crystal fraction of fluoride phase of $80SiO_2$-$20LaF_3$ sol-gel self-supported layers, resulted as high as 18 wt% of LaF_3; this is, up to our knowledge, the highest amount of active phase reported in literature.

Figures 4(d) shows the HRTEM images of self-supported layers of $20LaF_3$-$80SiO_2$ OxGCs, showing crystals of 8.0 nm after a heat-treated at 550 °C for 1 min and its corresponding size distribution. This crystal size is smaller than the one found for MQ materials (around 12 nm). Different from by MQ materials, where crystallization proceeds into the droplets formed during the nucleation, OxGCs produced by sol-gel present individual and well differentiated crystals homogenously distributed into the glass matrix.

Although, bulk or powder sol-gel samples present interesting optical results, thin films prepared from the same sols show very low luminescence efficiency likely due to the too small crystal size, around or below 2 nm [27,35]. The rapid densification of the silica matrix during the heat treatment inhibits the crystals growth resulting in low efficient glass-like optical response. [27] Many efforts are still needed to increase the crystal fraction and the crystal size in thin films obtained through this method.

In last years, an alternative route has been proposed that consists on the incorporation of a well-dispersed RE doped-NPs suspension into a sol-gel precursors solution. Cruz et al. [67] reported the synthesis of aqueous LaF_3 nanoparticles (NPs) suspension well dispersed in a SiO_2 sol. LaF_3-SiO_2 xerogels were obtained and heat-treated 6h at 450°C to eliminate the organic dispersant, polyvinylpyrrolidone (PVP) and densify the SiO_2 matrix. The shape of the LaF_3 NPs separated from the sol (Fig. 4(e)) obtained from the modified sol-gel synthesis is very different compared to the previously MQ and SG synthesis reported (Fig. 4(a) and (d)). Elongated nanoparticles, with an average size of 16nm were obtained.

Powders and thin films OxGCs have been prepared by this route with composition Nd^{3+}-doped $20LaF_3$-$80SiO_2$. XRD spectra confirmed the presence of LaF_3 as only phase in thin films and powders. Additionally, HRTEM analysis demonstrated that the incorporation of Nd^{3+}-doped LaF_3 NPs into the silica sol doesn't change their morphology either before or after heat-treatment.

Optical Materials EXPRESS

Table 1 summarizes the characteristics of the LaF_3 nanoparticles obtained by the different analysed methods as a function of synthesis process.

Table 1. Comparative of different hexagonal LaF_3 OxGCs prepared by MQ and SG. Lifetimes were obtained by exciting at 786 nm.

Process	Dopant (nominal mol.%)	mol.% Active phase	Shape of nanoparticles	Medium size of nanoparticles (nm)	τ_{exp}		References
					Room Temperature	Low Temperature	
MQ-bulk	$0.1Nd^{3+}$	<10%	Circular	11	604 µs	688 µs	[48]
	$0.1Nd^{3+}$	<10%	Circular	15	300 µs	Not reported	[71]
	$1Nd^{3+}$	<10%	Circular	15	98 µs	Not reported	[48]
MQ-fibres	$0.1Nd^{3+}$	<10%	Circular	14-15	608 µs	Not reported	[64]
	$2Nd^{3+}$	<10%	Circular	14-15	34 µs	Not reported	[64]
SG (TFA route)-bulk	$0.5Nd^{3+}$	20%	Circular	8	147 µs	Not reported	[68]
SG (TFA route)-thin film	$2Nd^{3+}$	20%	Circular	2.5	45 µs	Not reported	[68]
	$3Nd^{3+}$	20%	Circular	2.5	41 µs	Not reported	[68]
SG (Pre-crystallized nanoparticles route)-bulk	$0.9Nd^{3+}$ (mol.% respect to LaF_3)	20%	Elongated	16	528 µs	Not reported	[67]

3.2. Optical characterization

The first studies about OxGCs with lanthanides have been done for LaF_3, due to its low phonon energy and high solubility of rare earth ions. The most important applications of these materials focus on photonics and optical devices. Thus, it is crucial to compare the optical properties of these GCs and the efficiency of each processing method depending on the final material.

In the case of MQ [48], the optical properties of the 55Si10La glass composition, described in the section before, doped with 0.1-1 mol% NdF_3 were characterized by site-selective laser excitation along the $^4I_{9/2} \rightarrow {}^4F_{5/2}$ absorption band. Gorni et al. [48] reported that it is possible to obtain the emission spectrum of Nd^{3+} in LaF_3 NCs by exciting at 786 nm. As it is shown in Fig. 5(a), there is a strong difference in the $^4F_{3/2} \rightarrow {}^4I_{11/2}$ spectra under 786 nm and 802 nm excitation. The emission obtained by exciting at 786 nm shows a well resolved spectrum corresponding to Nd^{3+} in LaF_3 NCs whereas under 802 nm excitation an inhomogeneously broadened band similar to that of the glass sample is obtained. These spectra reveal that the Nd^{3+} is present in both crystalline and amorphous environments.

In order to minimize the spectral overlapping of the contributions from Nd^{3+} in the amorphous and crystalline phases the authors measured the emission spectra of the same samples at 9 K, enhancing the definition and sharpness of the peaks. As can be seen in Fig. 5(b) under 786 nm excitation, the spectrum shows sharp peaks, one of then at 1039 nm which does not overlap with the emission spectrum obtained at 802 nm. Under 802 nm excitation the spectrum is broader and similar to the glass sample. The results confirmed that under 786 nm excitation the emission corresponded to Nd^{3+} in the crystalline environment. The existence of two different environments for Nd^{3+} ions in the GCs was also confirmed by decay time measurements performed under excitation at 786 nm and 802 nm collecting the luminescence at 1039 nm and 1055 nm respectively (Fig. 5(c)). The decay obtained by exciting at 786 nm is single exponential with a lifetime of 688 µs corresponding to Nd^{3+} in the crystal environment, whereas at 802 nm the lifetime was 336 µs.

Gorni et al. [48] reported the emission, and excitation spectra and lifetimes for higher dopant concentrations and observed a clear decrease of the contribution of the Nd^{3+} emission in the

Optical Materials EXPRESS

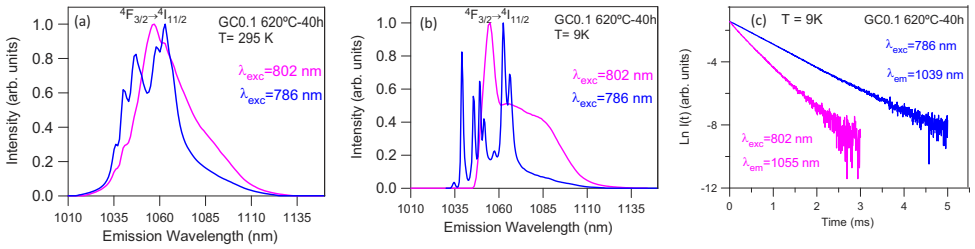

Fig. 5. Normalized emission spectra obtained by exciting at 786 and 802 nm for the GC 55Si10La with 0.1NdF_3 heat treated at 620 °C for 40 h corresponding to (a) 295 K, (b) 9 K and (c) Semilogaritmic plot of the experimental decays from the $^4F_{3/2}$ state obtained under 786 nm and 802 nm excitation at 9 K. *Adapted to* [48]*, copyright (2017), with permission form Elsevier.*

NCs together with a strong reduction of the lifetime from 688 µs to 98 µs when the concentration increased from 0.1 to 1%NdF_3. This behavior was attributed to the quenching generated by an excessive amount of dopant in the NCs due to a high diffusion of Nd^{3+} ions from the glass matrix to the LaF_3 nanocrystals. Using Rietveld refinement and XANES analysis to calculate the crystal fraction and the Nd^{3+} diffusion into the NCs, it was concluded that in the MQ samples doping the batch with a nominal concentration of 0.1 mol% NdF_3 results in an effective concentration of around 1 mol% in the NCs.

A similar behaviour was observed for Nd^{3+}-doped fibres OxGCs [64]. Lifetime measurements of the $^4F_{3/2}$ level at RT were performed under 786 nm excitation and a value of 608 µs was obtained. This value is similar to the one obtained at RT in bulk GCs samples by MQ and slightly lower than those measured at 9K probably due to thermal quenching.

The optical properties of Nd^{3+}-doped LaF_3 NCs were also studied in OxGCs prepared by SG following the TFA route. As shown in Fig. 6, when exciting at 9 K with λ_{exc} = 786 nm, the spectrum corresponding to the xerogel of 0.5Nd^{3+}-20LaF_3-80SiO_2 [68] shows an unstructured band, indicating an amorphous environment. Well-defined peaks appear related to the Nd^{3+} ions in the nanocrystals after heat-treatment at 650 °C for 3 h, with the same excitation. Quenching effect is observed when the dopant amount increases up to 3 mol% decreasing the lifetime of the $^4F_{3/2}$ state from 147 µs (0.5%) to 18 µs (3%).

The OxGCs with Nd^{3+} doped- LaF_3 NCs prepared by the pre-crystallized nanoparticles route of sol-gel were characterized by Cruz et al. [67] The emission spectrum recorded at RT at λ_{exc} = 786 nm of the LaF_3 NPs doped with 0.9Nd^{3+} heat treated at 450° C for 6 h (Fig. 7(a)) presents sharp peaks for the $^4F_{3/2}\rightarrow{}^4I_{11/2}$ transition indicating a crystalline environment. The lifetime of these NPs taken from the semi-logarithmic plot of the experimental decay under excitation at 786 nm collecting the luminescence at 1064 nm (Fig. 7(b)) shows a value of 528 µs similar to the one reported in literature for Nd^{3+} in LaF_3 crystal (522 µs) [69]. After the incorporation of the NPs to silica sol, a glass-ceramic with composition 0.9Nd^{3+}–80SiO_2:20LaF_3 was obtained. The corresponding aerogel does not show any luminescence emission, likely due to the presence of the organic dispersant (PVP). A heat treatment at 450 °C for 6 h has been done to eliminate the PVP from the dried sol. The emission obtained spectrum (Fig. 7(c)) depicts similar sharp peaks than those obtained from the heat treated nanoparticles, confirming that Nd^{3+} remains inside the NPs. The lifetime of 525 µs (Fig. 7(d)) is a further proof that NP maintain their optical efficiency after their incorporation in the silica matrix. These results are significantly different for those reported by MQ. Comparing the lifetimes obtained between MQ and sol-gel samples (98 µs by MQ and 528 µs by sol-gel for a high Nd^{3+} concentration around 1 mol%.), it is observed that the sol-gel samples are more efficient than the MQ. As mentioned before, the

Optical Materials EXPRESS

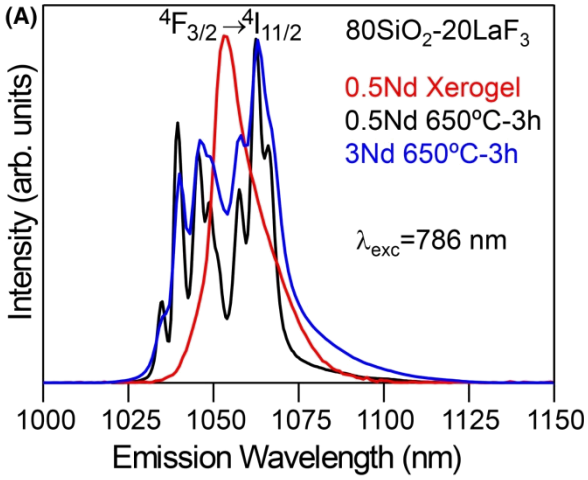

Fig. 6. Normalized emission spectra obtained at 9 K with λ_{exc} = 786 nm for 0.5 xerogel and 0.5 and 3% Nd^{3+}-$20LaF_3$-$80SiO_2$ GCs by SG. *Adapted from* [68], *copyright (2018)*.

effective Nd^{3+} concentration in MQ samples is much higher than the nominal one, which leads to concentration quenching.

Table 1 describes some characteristics of the LaF_3 OxGCs doped with Nd^{3+} obtained by MQ and SG together with the lifetimes obtained by exciting at 786 nm, corresponding to Nd^{3+} inside the nanocrystals. The lifetimes obtained under excitation at 786 nm by the pre-crystallized nanoparticles route of SG are promising (528 μs), much higher than those obtained by MQ for OxGCs with a similar Nd^{3+} concentration and analysed at 9 K with less active phase present (98 μs). (50) Other authors reported the optical properties of Nd^{3+} doped bulk OxGCs prepared by MQ. For example, Yu, Y. et al. [70] reported the preparation of bulk GCs with LaF_3 doped with $0.5Nd^{3+}$. The authors revealed a lifetime of 343 μs when exciting at λ_{exc} = 800nm. Others bulk OxGCs obtained by MQ are listed in the Table 1. [71] These values obtained for bulk materials by MQ are significantly higher than those found by TFA route of SG (147 μs). In the case of the "pre-crystallized nanoparticles route", the active phase fraction is similar to that of TFA. The change in the morphology and/or size of the nanoparticles can justify this improvement. In addition, a partial remain of RE ions in the matrix must be consider in the case of OxGCs obtained by TFA route. Kumar Sharma et al. [72] described the effect of the morphology of the host lattice on luminescence explaining that size, shape and surface defect play a vital role. Yang et al. [73] reported that in RE-doped EuF_3 nanoparticles, the emission found in nano-spindles is stronger than that from nano-disks and nano-columns.

In the case of LaF_3 nanocrystals in SG OxGCs, the particles with better efficiency are those prepared by pre-crystallized nanoparticles route of SG, with an average size of 16 nm, elongated shape and the nanoparticles found in OxGCs prepared by MQ, with medium size of 11 nm and circular planar shape. Thus, the goal to improve luminescence response implicates to increase the crystallinity of NP, control their morphology and identify further parameters responsible for lowering the optical efficiency.

Optical Materials EXPRESS

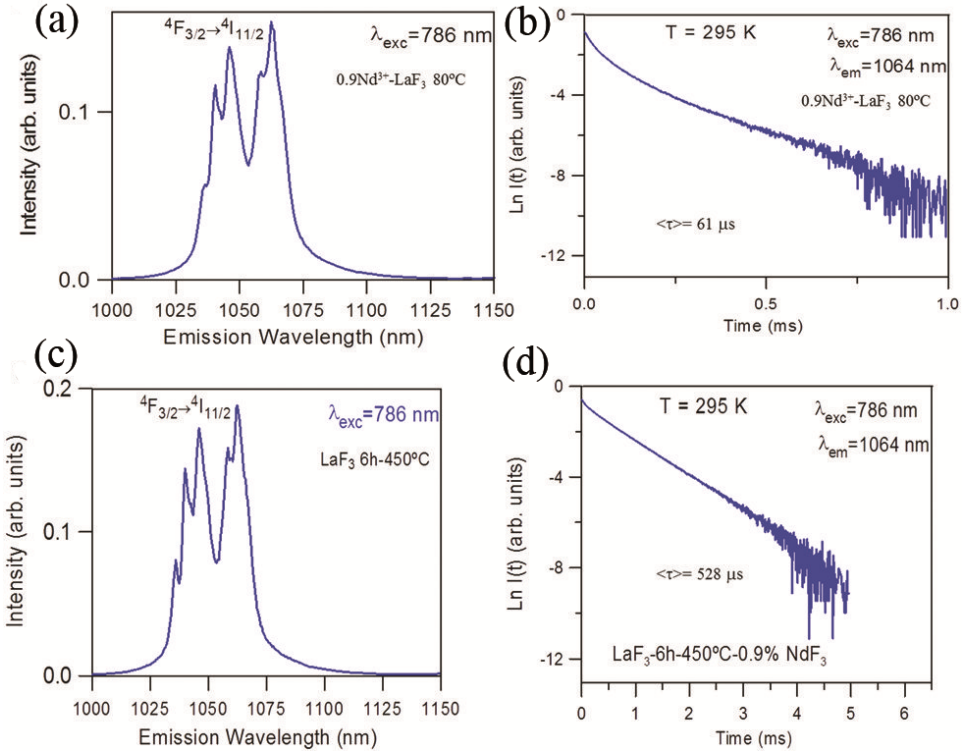

Fig. 7. (a) Room temperature emission spectrum of 0.9Nd^{3+}–LaF_3 nanoparticles treated at 80 °C obtained under excitation at 786 nm and (b) semi- logarithmic plot of the experimental decay obtained after excitation at 786 nm collecting the luminescence at 1064 nm. (c) Room temperature emission spectrum of 0.9Nd^{3+}–80SiO_2:20LaF_3 powder treated at 450 °C–6 h and (d) its corresponding semi-logarithmic plot of the experimental decay under excitation at 786 nm collecting the luminescence at 1064 nm. *Adapted from* [67], *copyright (2020).*

4. Comparative study of OxGCs containing $KLaF_4$ prepared by MQ, SPS and SG

Another relevant GCs are those constituted for a double fluoride crystalline phase such as $KLaF_4$. This phase can be present into two different polymorphs with different symmetry: cubic (α) and hexagonal (β). The most interesting phase in terms of optical efficiency is the β-$KLaF_4$, with a phonon energy of 260 cm^{-1}. Cornelis et al. [74] studied different double halides crystals, reporting that bigger ions such as K^+ in comparison to Na^+ lead to more stable crystals.

OxGCs with $KLaF_4$ nanocrystals has been reported for the first time by the GlaSS group in 2013, processed by MQ [18]. In 2018, Cabral et al [47] reported the presence of both phases in GCs doped with Nd^{3+} ions. In 2021, Cruz et al. [41] published for the first time OxGCs in the system $KLaF_4$ prepared by sol-gel and Babu et al. [33], by SPS technique. The following section compares the MQ, SPS and SG from the structural and optical characterisation details of the different final materials produced by these different techniques.

4.1. Structural characterization

de Pablos-Martin et al. [18,75] and Cabral et al. [47] prepared the composition 70 SiO_2 –7Al_2O_3–16K_2O–7LaF_3 (70Si7LaK) doped with xTm^{3+} - yYb^{3+} (x= 0.2 mol% of Tm_2O_3 and y= 0.5 mol% of YbF_3) and 0.1–2 mol% of NdF_3 respectively. Cubic (α) $KLaF_4$ nanocrystals were achieved for treatments at 580- 660°C. The authors assume an increase of the crystal fraction for

Optical Materials EXPRESS

longer heat treatment, due to the more defined XRD peaks. Crystal sizes remain around 9 nm for different heat-treatments, likely due to the high glass viscosity. Moreover, heat treatment at 600 °C and 660 °C permitted obtaining the hexagonal phase (β-$KLaF_4$) to be obtained, Fig. 8. The detection of β-$KLaF_4$ at higher temperatures from 55 h, allows assuming that the crystallization of this phase is not a polymorphic transformation, but derived from an earlier nucleation in the glass matrix, needing more temperature to grow. The authors also report different crystal growth rates for both phases, the crystallization kinetics of α and β phases being independent.

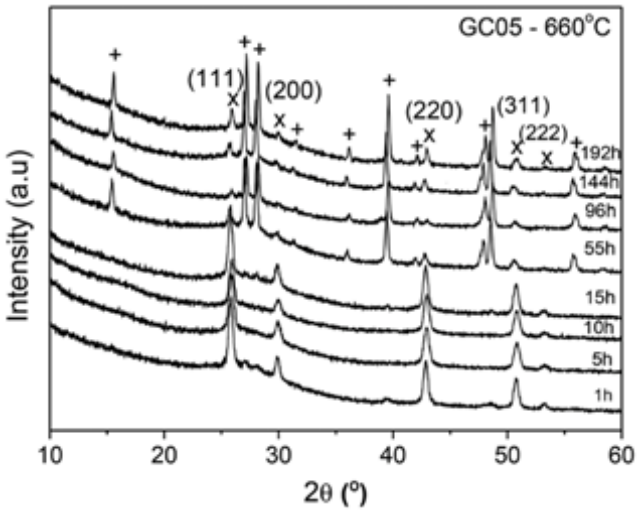

Fig. 8. XRD patterns for 0.5 mol%. NdF_3 -70Si7LaK GC sample treated at 660 °C at different times. (x): α-$KLaF_4$, (+): β- $KlaF_4$. Adapted from [47], copyright (2018).

Other important differences aroused from high definition XRD study of GCs 70Si7LaK doped with 0.1 Nd^{3+} and 0.5Nd^{3+} treated at 590 °C– 90 h. Figure 9(a) and (c) shows XRD patterns of 0.1Nd^{3+} - 70Si7LaK and 0.5Nd^{3+} - 70Si7LaK. For both, the presence of the α-$KLaF_4$ polymorph is observed. Although, in the case of the 0.5Nd^{3+} sample, the presence of the β-$KLaF_4$ polymorph with a crystal size of 11 nm is more evident. These results are confirmed by HR-TEM images (Fig. 9(b) and (d)), where the presence of two different d-space, 0.56 nm and 0.34 nm, indicate that planes [100] and [111] corresponding with β- $KLaF_4$ and α- $KLaF_4$, respectively. A similar study was performed on GCs doped 0.1 mol% Nd^{3+}, which XRD patterns are depicted in Fig. 9(a), where only few low-intensity peaks β- $KLaF_4$ appear. The nanocrystals size corresponds to 9 and 11 nm for α- $KLaF_4$ and β- $KLaF_4$ polymorphs respectively. Only α- $KLaF_4$ polymorph can be detected by TEM, with d-spacing, 0.21 and 0.33 nm, corresponding to planes [220] and [111], respectively.

GlaSS group also prepared $KLaF_4$ OxGCs using SPS method [33]. The composition was the same produced by MQ and doped with xNdF_3 (mol%, x= 0.1, 0.5 and 1.0 mol%). SPS GCs samples were sintered under vacuum conditions at temperature 700 °C, pressure 22 MPa and holding time of 20 min. Although, the samples were protected with a platinum foil some signals of carbon contamination remain. For particles sizes between 100- 63 μm, authors showed the obtention of the most transparent samples as can be seen in Fig. 10.

The XRD patterns obtained at different holding times and particle sizes (Fig. 11) show α-$KLaF_4$ (JCPDS 075 2020) as the only phase present independently of dopant concentration. It is demonstrated that crystallization and crystal size increase with increasing treatment-time and precursor particle size.. This is due that large particle size that avoids the deposition of carbon in the porous during the viscous sintering, as can be described in [33].

Optical Materials EXPRESS

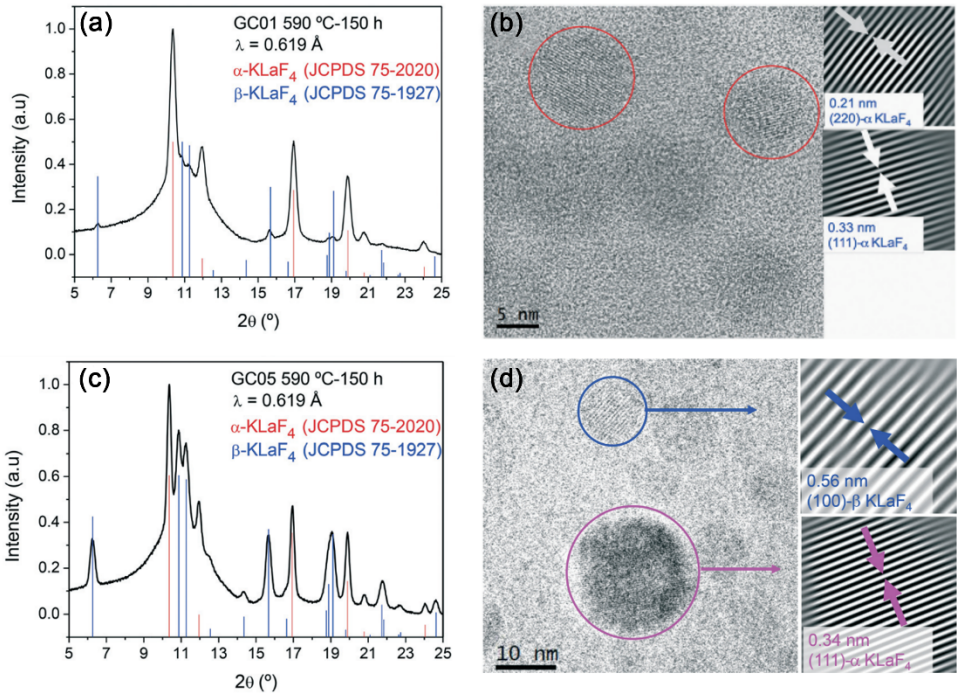

Fig. 9. (a) and (c) show XRD patterns of GCs $KLaF_4$ doped with 0.1 and 0.5 mol% of Nd^{3+} respectively, at BM25- Spline of ESRF. (b) and (d) HR-TEM images showing a detail of α and β crystals with the corresponding plane distance of the same samples, treated at 590 °C–150 h. Adapted from [47], copyright (2018).

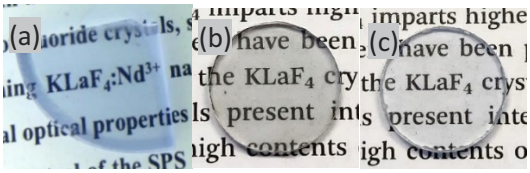

Fig. 10. Comparative image between (a) MQ glass piece, (b) and (c) SPS-GCs $KLaF_4$:0.5Nd^{3+} obtained at 700 °C, 20 min with particle size x< 63 μm and 100 < x< 63 μm respectively. *Adapted from* [33], *copyright (2021), with permission from Elsevier.*

Optical Materials EXPRESS

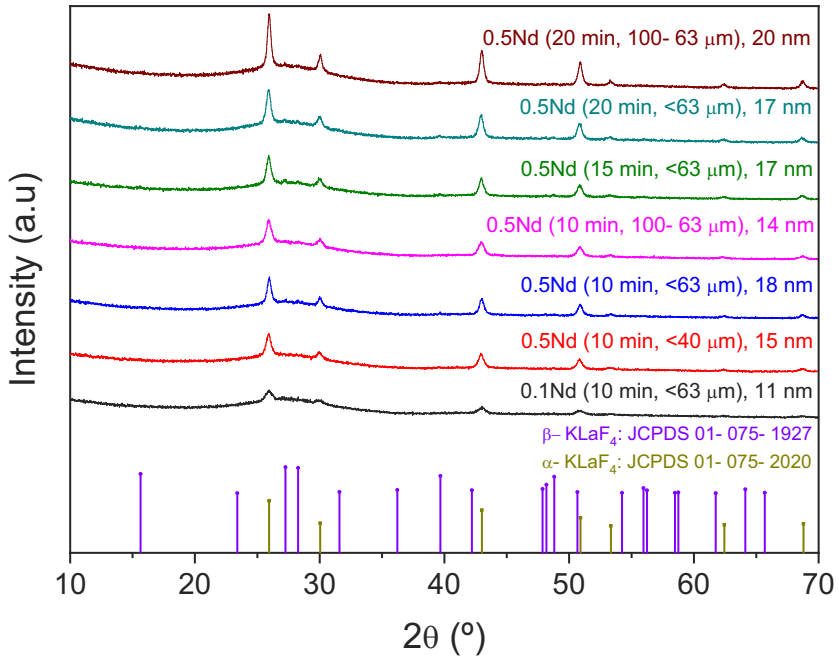

Fig. 11. XRD patterns of $KLaF_4$ SPS GCs doped with 0.1 and 0.5 NdF_3 starting from different particle size powders and with different holding times of the SPS experiment at 700 °C. *Adapted from* [33], *copyright (2021), with permission from Elsevier*.

When comparing these results with those of similar materials prepared by MQ and sol-gel, the most important issue is the absence of β- $KLaF_4$ phase in SPS GCs samples. S. Babu et al. [33] suggests that after longer treatment times, β- $KLaF_4$ could be potentially achieved but this eliminate one major advantages of SPS over other processing methods.

The structural characterization of these SPS GCs was complemented with HR-TEM. The results confirm show that the average crystal size for the $0.5Nd^{3+}$ sample was 15 nm, very similar to that obtained by XRD (not shown).

The phase $KLaF_4$ has been also prepared by sol-gel method for the first time by the GlaSS group [41]. Two compositions, $10KLaF_4$-$90SiO_2$ and $20KLaF_4$-$80SiO_2$ have been studied. DTA analysis of $20KLaF_4$-$80SiO_2$ system reveals a crystallization peaks around 300 °C, similar to LaF_3-SiO_2 system. XRD were performed for both compositions, $10KLaF_4$-$90SiO_2$ and $20KLaF_4$-$80SiO_2$, for 1min at 550 °C, and also from 450 °C to 650 °C only for the composition $20KLaF_4$-$80SiO_2$. For the lower content of crystal phase $10KLaF_4$-$90SiO_2$, α- $KLaF_4$ has only appeared. Figure 12 shows the XRD evolution of $20KLaF_4$-SiO_2 system as a function of temperature, from 350 °C to 650 °C. Defined peaks of α- $KLaF_4$ appear at 350 °C, while β- $KLaF_4$ (hexagonal phase) becomes the major phase over 550 °C. The crystal size was calculated by XRD; α-$KLaF_4$ nanocrystals increase with increasing temperature from 350 °C to 650 °C, from 12 nm to 19 nm, maintaining stable for higher T. Although, the hexagonal phase maintains a near constant size of 16 nm and 17 nm for 550 °C and 650 °C heat treatment. These results were confirmed by HRTEM, finding a medium diameter of 16 nm for $20KLaF_4$-SiO_2. The crystal fraction of each phase for the GCs $20KLaF_4$-SiO_2 treated at 550 °C for 1 min was also calculated by Rietveld Refinement, obtaining 75% of crystalline phase corresponding to hexagonal (β) $KLaF_4$.

Optical Materials EXPRESS

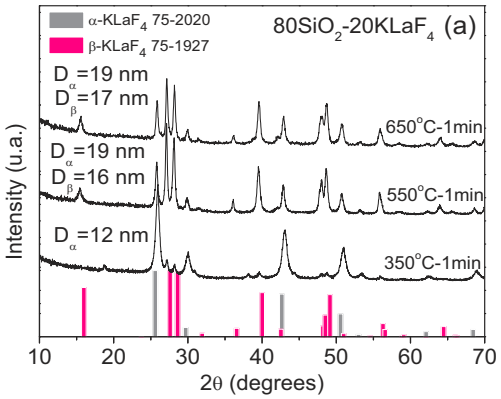

Fig. 12. XRD patterns for GC sample $20KLaF_4$-$80SiO_2$ treated at 350, 550 and 650 °C for 1 min. *Adapted to* [41], *copyright (2021), with permission from Elsevier*.

These results are quite different from those of MQ materials where α-$KLaF_4$ is the predominant phase. The crystal size obtained by SG is slightly similar than that obtained by MQ (9 nm and 11 nm respectively) and to those obtained by SPS for the same concentration (11 nm). From these results it seems clear that SG represent a great advantage respecting to MQ and SPS for preparing $KLaF_4$ OxGC, since it permits obtaining the more efficient β-phase, as well as higher contents of active crystal phase with suitable crystal size.

4.2. Optical characterization

Respect to the optical characterization, A. Cabral et al. [47] used site-selective laser spectroscopy on $KLaF_4$ GCs obtained by MQ, explained in the section before, showing that Nd^{3+} ions are incorporated in both crystalline phases, α-$KLaF_4$ and β-$KLaF_4$. To avoid the overlapping of the contribution of the Nd^{3+} both in crystalline and amorphous environment, the authors measured the emission and excitation spectra and lifetimes at low temperatures (4.2 K). The $^4F_{3/2} \rightarrow {}^4I_{11/2}$ emission spectra, shown in Fig. 13(a), of OxGCs with composition 70Si7LaK with 0.1 mol.% Nd^{3+} were recorded under excitation at 792 nm and 801 nm (the excitation wavelengths assigned to the β-$KLaF_4$ and α-$KLaF_4$ phases respectively based on the low temperature excitation spectra) (49). Under 792 nm excitation, the spectrum presents a broad band, similar to those of a glass environment confirming the very low contribution of Nd^{3+} in the β-$KLaF_4$ NCs. A more defined peak is obtained when exciting at $\lambda_{exc} = 801$ nm, as shown in Fig. 13(a). However, when the content of Nd^{3+} was increased to 0.5%Nd^{3+}, under both excitation wavelengths the spectra show a sharp peak together with a structured band (Fig. 13(b)). This result indicates that when the content of neodymium was increased from 0.1 to 0.5, the contribution of the β-$KLaF_4$ also increased. These results are in concordance to that obtained in XRD by Cabral et al. [47], shown in the section before in Fig. 9.

Decay curves were recorded for 0.1, 0.5 and 1% Nd^{3+} GCs, at low temperatures (4.2K) exciting the $^4F_{5/2}$ level at 792 nm and 801 nm and collecting the luminescence at 1046 nm. Curves recorded with the emission collected at 1046nm and excited at $\lambda_{exc} = 801$ nm reveal a lifetime of 494 μs and 423 μs for the GC with 0.1 mol% Nd^{3+} and 1 mol% Nd^{3+}, respectively. These lifetimes values are associated to the α-$KLaF_4$ phase which is the main crystalline phase for these concentrations. Cabral et al. [47] reported than when the samples were excited at another excitation wavelengths along the $^4I_{9/2} \rightarrow {}^4F_{5/2}$ absorption band, the decay curves were deviated from a single exponential function, due to the overlapping of the emission from the two crystalline (α and β) and amorphous phases, and the lifetime values ranged between 535 μs and 466 μs for

Optical Materials EXPRESS

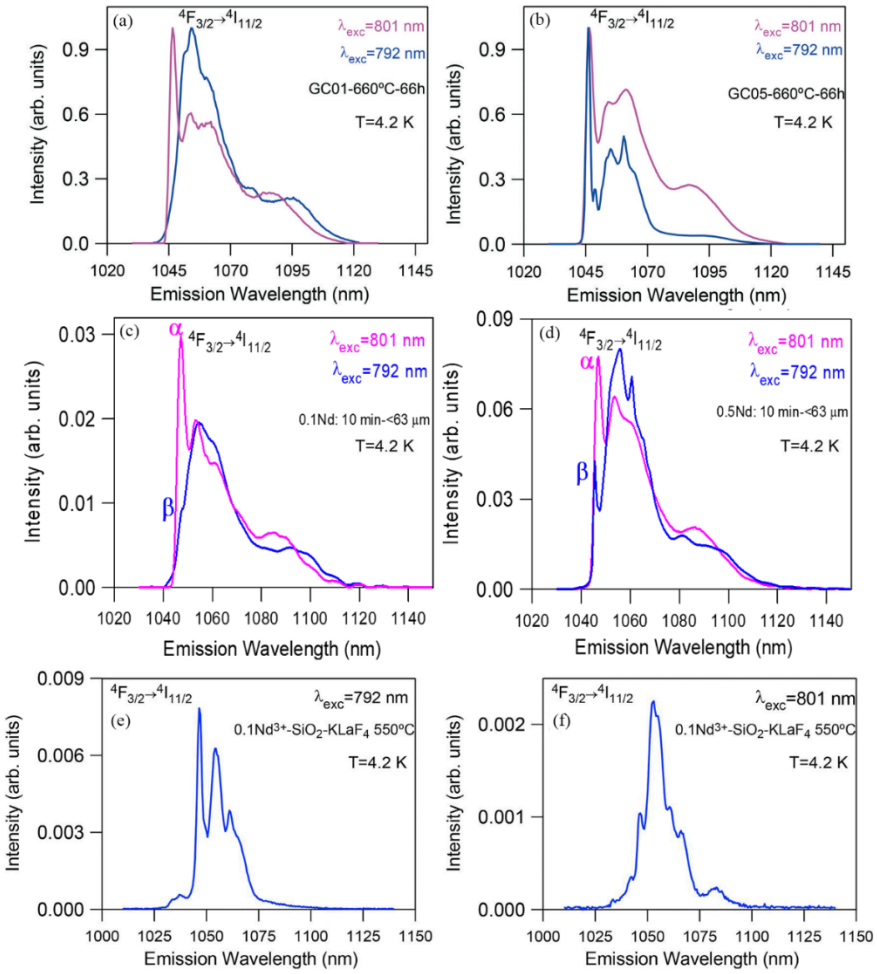

Fig. 13. (a) and (b) Low temperature (T= 4.2 K) normalized emission spectra obtained by exciting at 792 nm and 801 nm for the OxGCs prepared by MQ 70Si7LaK with 0.1 mol% Nd^{3+} and 0.5 mol% Nd^{3+}. *Adapted from* [47], *copyright (2018)*. (c) and (d) Low temperature (T= 4.2 K) normalized emission spectra obtained by exciting at 792 and 801 nm for SPS GCs doped with 0.1 and 0.5 mol% Nd^{3+} respectively. *Adapted from* [33], *copyright (2021), with permission from Elsevier*. (d) and (e) Low temperature emission spectra corresponding to the Nd^{3+} $^4F_{3/2}\rightarrow{}^4I_{11/2}$ laser transition obtained under excitation at 792 and 801 nm for the GC sample prepared by SG. *Adapted from* [41], *copyright (2021), with permission from Elsevier*.

the sample doped with 0.1% and between 429 µs to 335 µs for 1% GC sample. In the case of the GC sample doped with 0.5%, only under 792 nm excitation the decay was well described by a single exponential function with a lifetime of 440 µs attributed to the lifetime of the β-$KLaF_4$ crystalline phase.

On the other hand, Babu et al. [33] studied the optical properties of the samples prepared by SPS, described before in the present work. The results confirmed the presence of Nd^{3+} ions in both crystalline and amorphous phases for 0.1 and 0.5 Nd^{3+} samples. The emission spectra, recorded at 4.2 K, performed by exciting at 792 nm and 801 nm (Fig. 13(c) and (d)) showed the emission of Nd^{3+} in the α-$KLaF_4$ phase as predominant. The low contribution of the

Optical Materials EXPRESS

hexagonal phase is confirmed by the spectrum obtained at $\lambda_{exc} = 792$ nm, which shows a broad band similar to the glass sample with a small feature around 1046 nm, in agreement with the structural characterization. In $0.5Nd^{3+}$ doped samples, the spectrum recorded under $\lambda_{exc} = 792$ nm, the excitation wavelength assigned to the β-$KLaF_4$ phase, shows a sharp peak at 1046 nm together with a structured band, similar to that reported by MQ. However, the intensity of this peak is lower than those obtained in materials prepared by MQ, indicating a smaller amount of beta phase in SPS samples. Under 801 nm excitation the spectra show similar features for both samples with a narrow peak at 1047 nm (attributed to Nd^{3+} ions occupying α -$KLaF_4$ crystalline phase) together with a broad band. The lifetimes values obtained at low temperature (4.2 K) for samples 0.1 and 0.5 Nd^{3+} were 475 μs ($\lambda_{exc} = 792$ nm) and 478 μs ($\lambda_{exc} = 801$ nm) for the sample doped with 0.1% and 391 μs ($\lambda_{exc} = 792$ nm) and 403 μs ($\lambda_{exc} = 801$ nm) for the 0.5% sample. In this case, due to the spectral overlap of the emission of both crystalline phases and the predominance of α-$KLaF_4$ phase in all samples, the authors cannot unambiguously conclude that the lifetime obtained under 792 nm excitation corresponds to the β-$KLaF_4$ phase.

Cruz et al. [41] also reported the luminescence behaviour of sol-gel $0.1Nd^{3+}$-$20KLaF_4$-$80SiO_2$ GCs prepared by TFA route and containing higher amount of hexagonal phase. The excitation spectra of the emission at 1046 nm presents a sharp intense peak at 792 nm together with a less intense and broader peak at 801 nm, also observed in MQ samples, confirming the presence of both α and β $KLaF_4$ phases. Figures 13(e) and (f), depict the emission related to excitation at 792 nm, with peaks well resolved and defined, losing definition when excited at 801 nm. This

Table 2. Comparison of different $KLaF_4$ OxGCs prepared by MQ, SPS and SG (λ_{exc} (α-$KLaF_4$) 801 nm, λ_{exc} (β-$KLaF_4$)= 792 nm).

Process	Crystal phase	Dopant	Active phase (mol%)	Shape of nanoparticles	Average size of nanoparticles (nm)	τ_{exp} (Low temperature)	
MQ-Bulk	α-$KLaF_4$ and β-$KLaF_4$	0.1 Nd^{3+}	<10%	Circular	9 and 11 respectively	494 μs (λexc = 801 nm)	[47]
	α-$KLaF_4$ and β-$KLaF_4$	0.5 Nd^{3+}	<10%	Circular	20 and 11 respectively	440 μs (λexc= 792nm)	[47]
	α-$KLaF_4$ and β-$KLaF_4$	1 Nd^{3+}	<10%	Circular	Not reported	423 (λexc= 801nm)	[47]
SPS-GCs-bulk	α-KLaF4 and β-KLaF4	0.1 Nd^{3+}	<10%	Circular	11	475μs (λexc= 792nm)	[33]
	α-KLaF4 and β-KLaF4	0.1 Nd^{3+}	<10%	Circular	11	478μs (λexc= 801nm)	[33]
	α-$KLaF_4$ and β-$KLaF_4$	0.5Nd^{3+}	<10%	Circular	15	391μs ((λexc= 792nm)	[33]
	α-$KLaF_4$ and β-$KLaF_4$	0.5Nd^{3+}	<10%	Circular	15	403 μs (λexc= 801nm)	[33]
SG (TFA route)-bulk	α-$KLaF_4$ and β-$KLaF_4$	0.1Nd^{3+}	20%	Circular	19	538 μs ((λexc= 792nm)	[41]
	α-$KLaF_4$ and β-$KLaF_4$	0.1Nd^{3+}	20%	Circular	16	508 μs (λexc= 801nm)	[41]

Optical Materials EXPRESS

different behaviour is probably due to a higher amount of β-$KLaF_4$ phase, excited at $\lambda_{exc} = 792$ nm, respecting to α-$KLaF_4$. Moreover, the lifetime obtained by SG for an excitation of 801 nm, corresponding to α-$KLaF_4$, was 508 μs, similar to MQ, 494 μs.

The results obtained for the three types of processing show that the highest β-phase content is achieved by sol-gel.

Table 2 summarizes the results obtained by MQ, SPS and sol-gel for the OxGCs containing $KLaF_4$ as active phase (λ_{exc} (α-$KLaF_4$)= 801 nm, λ_{exc} (β-$KLaF_4$)= 792 nm). In the samples obtained by MQ and SPS, the active phase is less than 10% while in samples obtained by sol-gel process this active phase is between 10- 20%. For all processing methods the shape of nanoparticles are circular and the presence of β-$KLaF_4$ phase is observed. Nevertheless, for SPS samples, the presence of hexagonal phase was too small to be correctly identified. By sol-gel is possible to get larger crystals of β-$KLaF_4$ phase than for MQ.

In conclusion, it can be said that in the case of needing the presence of a large amount of β-$KLaF_4$ phase in relatively short times, sol-gel processing is a great option. However, with sol-gel is difficult obtaining bulk material, so if it is required the presence of β-$KLaF_4$ phase in a bulk melt-quenching is the option, although long times are required. On the other hand, SPS requires shorter times, but the α-$KLaF_4$ crystalline phase is dominant with this type of processing.

5. General conclusion and perspectives

Transparent oxyfluoride glass-ceramics have been developed for the last decades with promising results in their optical properties. The processing method by which these materials can be obtained is determinant for their further application. Three different processes have been described in this work, MQ, SPS and SG. Melt-quenching demonstrated to be the most suitable process for preparing bulk and fiber OxGCs with high optical efficiency despite the uncontrollable content of active phase due to the fluoride losses. As an alternative for the bulk OxGCs obtention, SPS is being developed. Only few work of SPS has been reported, the results demonstrate that is suitable for photonic applications as the lifetimes reported are encouraging, very similar to those obtained by MQ with the same compositions. Improving the content of active phase, sol-gel appeared as a suitable process for OxGCs bulk, powders and films. Compositions with more than 20% of fluorides have been described and the optical results demonstrated the higher efficiency of these materials. Although 20% it is considered as a high amount of active phase, it is necessary to continue studying the incorporation of more content of fluorides into the glass matrix. In addition, the pre-crystallized nanoparticle route described in this work is a promising method to prepare OxGCs coatings but at the moment only a few articles have been published about it and it is a challenge for the next years to go deep on this process. In this research the finding of an appropriate dispersant and the design of a suitable heat treatment for the coatings would be the most important goals.

All the OxGC materials obtained by MQ described in this article are suitable for preparing preforms as precursors for drawing optical fibres, as well as substrates for waveguides written using laser radiation. First attempts were successful and published in Refs. [25,76]. Further work is in progress to identify the structural changes caused by the interaction of the glass-ceramic with the laser and improve the quality of the waveguides.

On the other hand, it is well known that the addition of Ag ions can efficiently enhance the luminescent properties in RE-doped glasses. Ag resides in the glass as isolated Ag^+ ions, molecular-line Ag nanoclusters, or Ag NPs with surface plasmonic resonance (SPR) absorption bands [77–79]. In particular, the fluorescent enhancement of Ag NPs is due to the increase in the electromagnetic field that surrounds them. The spectroscopic properties of these materials have been studied in visible and near-infrared ranges [80,81] but not so much in the mid-infrared (MIR). The MIR emission is particularly important because most molecules display a high absorption

Optical Materials EXPRESS

cross-section in this region and therefore these materials present promising applications in chemical and biomolecular sensing and food-quality control [82]. An important goal is the preparation of oxyfluoride transparent GCs containing Ag, Au and Pt NPs doped with RE ions such as Eu, Nd, Er and Er/Yb to further enhance the luminescent response.

An important target is also to prepare new GCs by SPS; in particular, a main objective is to employ SPS for processing glass matrix composites by mixing glass powder, obtained by MQ, with NPs of fluoride phases obtained by SG. The glass matrix can either crystallize the same fluoride phase of the incorporated NPs during the SPS experiment or remain amorphous. For this purpose, various glasses from different glass systems, including not only oxyfluorides but borosilicate or borate compositions, which present lower processing temperatures, are being considered. A main advantage is that the amount of NPs to be incorporated and its crystallization degree may be controlled. Moreover, the dopant concentration could only be present in the SG-synthesized NPs and not in the glass matrix, avoiding emissions from the glassy phase.

This should be a more efficient method respecting to others preparing hybrid glasses, by incorporating the NPs that are produced in the melted glass at high temperature (temperature also dependent on the glass system) that lead to a significant dissolution of the particles [83,84]. The glass systems must necessarily present very low melting temperatures, such as phosphates, borates or tellurites, to maintain particle integrity. SPS method and low processing temperatures favour the preparation of transparent materials which maintain the structure and integrity of the NPs and their localization in the more stable and refractory glass matrices. Additionally, this type of processing will allow hybrid materials with crystalline lithium double fluorides to be prepared, otherwise very difficult to obtain by the conventional glass-ceramic route. These double fluorides may be obtained by the SG method, but the sintering process by SPS of these hybrid materials needs important development to get optimised mixtures of glass powder and NPs prepared in wet media, followed by drying and consolidation of the green pieces or layer of a certain thickness. The various steps constitute a challenge for future investigations.

Funding. MICINN (PID2020-115419GB-C-21/C-22).

Acknowledgments. The authors acknowledge financial support from MICINN under project PID2020-115419GB-C21/C-22/AEI/10.13039/501100011033. This article is a part of dissemination activities of the project FunGlass, which has received funding from the European Unionś Horizon 2020 research and innovation program under grant agreement No 739566.

Disclosures. The authors declare no conflicts of interest.

Data availability. No data were generated or analyzed in the presented research.

References

1. J. Deubener, M. Allix, M.J. Davis, A. Duran, T. Höche, T. Honma, T. Komatsu, S. Krüger, I. Mitra, R. Müller, S. Nakane, M.J. Pascual, J.W.P. Schmelzer, E.D. Zanotto, and S. Zhou, "Updated definition of glass-ceramics," J. Non-Cryst. Solids **501**, 3–10 (2018).
2. R. K. Sharma, A.V. Mudring, and P. Ghosh, "Recent trends in binary and ternary rare-earth fluoride nanophosphors: How structural and physical properties influence optical behavior," J. Lumin. **189**, 44–63 (2017).
3. T. Grzyb and S. Lis, "Photoluminescent properties of LaF_3:Eu^{3+} and GdF_3:Eu^{3+} nanoparticles prepared by co-precipitation method," J. Rare Earths **27**(4), 588–592 (2009).
4. Y. Wang and J. Ohwaki, "New transparent vitroceramics codoped with Er3+ and Yb3+ for efficient frequency upconversion New transparent vitroceramics frequency upconversion," 3268, 22–25 (1993).doi:10.1063/1.110170.
5. X. Liu, J. Zhou, S. Zhou, Y. Yue, and J. Qiu, "Transparent glass-ceramics functionalized by dispersed crystals," Prog. Mater. Sci. **97**, 38–96 (2018).
6. R.M. Almeida and M.C. Gonçalves, "Crystallization of Solgel-Derived Glasses," Int. J. Appl. Glass Sci. **5**(2), 114–125 (2014).
7. P. P. Fedorov, A. A. Luginina, and A. I. Popov, "Transparent oxyfluoride glass ceramics," J. Fluorine Chem. **172**, 22–50 (2015).
8. J. J. Velázquez, J. Mosa, G. Gorni, R. Balda, J. Fernández, A. Durán, and Y. Castro, "Novel sol-gel SiO_2-$NaGdF_4$ transparent nano-glass-ceramics," J. Non-Cryst. Solids **520**, 119447 (2019).
9. L. Li, F. Wang, Q. Liao, Y. Wang, H. Zhu, and Y. Zhu, "Synthesis of phosphate based glass-ceramic waste forms by a melt-quenching process: The formation process," J. Nucl. Mater. **528**, 151854 (2020).

Optical Materials EXPRESS

10. H. Lee, S. H. Lee, Y. G. Choi, W. Bin Im, and W. J. Chung, "Eu^{2+} and Mn^{2+} co-doped oxyfluoride glass ceramic for white color conversion of 400 nm UV-LED," J. Lumin. **222**, 117156 (2020).
11. A. De Pablos-Martín, A. Durán, and M. J. Pascual, "Nanocrystallisation in oxyfluoride systems: Mechanisms of crystallisation and photonic properties," Int. Mater. Rev. **57**(3), 165–186 (2012).
12. A. de Pablos-Martín, J. Méndez-Ramos, J. Del-Castillo, A. Durán, V. D. Rodríguez, and M. J. Pascual, "Crystallization and up-conversion luminescence properties of Er^{3+}/Yb^{3+}-doped $NaYF_4$-based nano-glass-ceramics," J. Eur. Ceram. Soc. **35**(6), 1831–1840 (2015).
13. R. Lisiecki and W. Ryba-Romanowski, "Silica-based oxyfluoride glass and glass-ceramic doped with Tm^{3+} and Yb^{3+} -VUV-VIS-NIR spectroscopy and optical thermometry," J. Alloys Compd. **814**, 152304 (2020)..
14. Y. Peng, J. Zhong, X. Li, J. Chen, J. Zhao, X. Qiao, and D. Chen, "Controllable competitive nanocrystallization of La^{3+}-based fluorides in aluminosilicate glasses and optical spectroscopy," J. Eur. Ceram. Soc. **39**(4), 1420–1427 (2019).
15. M.J. Dejneka, "The luminescence and structure of novel transparent oxyfluoride glass-ceramics," 239, 149–155 (1998).
16. J. K. Cao, X. Y. Wang, X. M. Li, Y. Le Wei, L. P. Chen, and H. Guo, "Enhanced emissions in Tb^{3+}-doped oxyfluoride scintillating glass ceramics containing KLu_2F_7 nano-crystals," J. Lumin. **170**, 207–211 (2016).
17. A. De Pablos-Martín, N. Hémono, G. C. Mather, S. Bhattacharyya, T. Höche, H. Bornhöft, J. Deubener, F. Muñoz, A. Durán, and M. J. Pascual, "Crystallization kinetics of LaF_3 nanocrystals in an oxyfluoride glass," J. Am. Ceram. Soc. **94**(8), 2420–2428 (2011).
18. A. De Pablos-Martín, F. Muñoz, G. C. Mather, C. Patzig, S. Bhattacharyya, J. R. Jinschek, T. Höche, A. Durán, and M. J. Pascual, "$KLaF_4$ nanocrystallisation in oxyfluoride glass-ceramics," CrystEngComm **15**(47), 10323–10332 (2013).
19. D. Chen, Z. Wan, Y. Zhou, P. Huang, J. Zhong, M. Ding, W. Xiang, X. Liang, and Z. Ji, "Bulk glass ceramics containing Yb^{3+}/Er^{3+}: β-$NaGdF_4$ nanocrystals: Phase-separation-controlled crystallization, optical spectroscopy and upconverted temperature sensing behavior," J. Alloys Compd. **638**, 21–28 (2015).
20. M. Secu and C. E. Secu, "Up-conversion luminescence of Er^{3+}/Yb^{3+} co-doped $LiYF_4$ nanocrystals in sol-gel derived oxyfluoride glass-ceramics," J. Non-Cryst. Solids **426**, 78–82 (2015).
21. A. De Pablos-Martín, M. O. Ramírez, A. Durán, L. E. Bausá, and M. J. Pascual, "Tm^{3+} doped oxy-fluoride glass-ceramics containing $NaLaF_4$ nano-crystals," Opt. Mater. (Amsterdam, Neth.) **33**(2), 180–185 (2010).
22. E. Elsts, G. Krieke, U. Rogulis, K. Smits, A. Zolotarjovs, J. Jansons, A. Sarakovskis, and K. Kundzins, "Rare earth doped glass–ceramics containing $NaLaF_4$ nanocrystals," Opt. Mater. (Amsterdam, Neth.) **59**, 130–135 (2016).
23. E. Augustyn, M. Zelechower, D. Stróz, and J. Chrapoński, "The microstructure of erbium-ytterbium co-doped oxyfluoride glass-ceramic optical fibers," Opt. Mater. (Amsterdam, Neth.) **34**(6), 944–950 (2012).
24. K.V. Krishnaiah, Y. Ledemi, E.S. de Lima Filho, G. Nemova, Y. Messaddeq, and R. Kashyap, "Ytterbium-doped oxyfluoride nano-glass-ceramic fibers for laser cooling," Work. Spec. Opt. Fibers Their Appl. WSOF 2015 **7**, WW3A.5 (2015).
25. G. Gorni, J. J. Velázquez, M. Kochanowicz, D. Dorosz, R. Balda, J. Fernández, A. Durán, and M. J. Pascual, "Tunable upconversion emission in $NaLuF_4$-glass-ceramic fibers doped with Er^{3+} and Yb^{3+}," RSC Adv. **9**(54), 31699–31707 (2019).
26. G. Lakshminarayana, E. M. Weis, A. C. Lira, U. Caldiño, D. J. Williams, and M. P. Hehlen, "Cross Relaxation in rare-earth-doped oxyfluoride glasses," J. Lumin. **139**, 132–142 (2013).
27. G. Gorni, J. J. Velázquez, J. Mosa, G. C. Mather, A. Serrano, M. Vila, G. R. Castro, D. Bravo, R. Balda, J. Fernández, A. Durán, and Y. Castro, "Transparent sol-gel oxyfluoride glass-ceramics with high crystalline fraction and study of re incorporation," Nanomaterials **9**(4), 530 (2019)..
28. B. Singarapu, D. Galusek, A. Durán, and M.J. Pascual, "Glass-ceramics processed by spark plasma sintering (SPS) for optical applications," Appl. Sci. **10**(8), 2791 (2020).
29. F. Al Mansour, N. Karpukhina, S. Grasso, R. M. Wilson, M. J. Reece, and M. J. Cattell, "The effect of spark plasma sintering on lithium disilicate glass-ceramics," Dent. Mater. **31**(10), e226–e235 (2015).
30. G. Delaizir, M. Dollé, P. Rozier, and X. H. Zhang, "Spark plasma sintering: An easy way to make infrared transparent glass-ceramics," J. Am. Ceram. Soc. **93**(9), 2495–2498 (2010).
31. P. Riello, S. Bucella, L. Zamengo, U. Anselmi-Tamburini, R. Francini, S. Pietrantoni, and Z.A. Munir, "Erbium-doped LAS glass ceramics prepared by spark plasma sintering (SPS)," J. Eur. Ceram. Soc. **26**(15), 3301–3306 (2006).
32. A. Bertrand, J. Carreaud, G. Delaizir, J. R. Duclère, M. Colas, J. Cornette, M. Vandenhende, V. Couderc, and P. Thomas, "A comprehensive study of the carbon contamination in tellurite glasses and glass-ceramics sintered by spark plasma sintering (SPS)," J. Am. Ceram. Soc. **97**(1), 163–172 (2014).
33. S. Babu, R. Balda, J. Fernández, M. Sedano, G. Gorni, A. A. Cabral, D. Galusek, A. Durán, and M. J. Pascual, "$KLaF_4$:Nd^{3+} doped transparent glass-ceramics processed by spark plasma sintering," J. Non-Cryst. Solids **578**, 121289 (2022)..
34. S. Fujihara, M. Tada, and T. Kimura, "Sol-Gel Processing of LaF_3 Thin Films," J. Ceram. Soc. Jpn. (Jpn. Ed., 1988-1991) **106**(1229), 124–126 (1998).
35. S. Fujihara, C. Mochizuki, and T. Kimura, "Formation of LaF_3 microcrystals in sol-gel silica," J. Non-Cryst. Solids **244**(2-3), 267–274 (1999).

Optical Materials EXPRESS

36. S. Georgescu, A. M. Voiculescu, C. Matei, C. E. Secu, R. F. Negrea, and M. Secu, "Ultraviolet and visible up-conversion luminescence of Er^{3+}/Yb^{3+} co-doped CaF_2 nanocrystals in sol-gel derived glass-ceramics," J. Lumin. **143**, 150–156 (2013).
37. D. Chen, Y. Wang, Y. Yu, E. Ma, and L. Zhou, "Microstructure and luminescence of transparent glass ceramic containing Er^{3+}:BaF_2 nano-crystals," J. Solid State Chem. **179**(2), 532–537 (2006).
38. N. Pawlik, B. Szpikowska-Sroka, T. Goryczka, M. Zubko, J. Lelątko, and W. A. Pisarski, "Structure and luminescent properties of oxyfluoride glass-ceramics with YF_3:Eu^{3+} nanocrystals derived by sol-gel method," J. Eur. Ceram. Soc. **39**(15), 5010–5017 (2019).
39. X. Wang, S. Fujihara, T. Kimura, and H. Chen, "Crystal structures of $BaMgF_{4-x}O_{x/2}$ thin films," Ferroelectrics **264**(1), 121–126 (2001).
40. G. Gorni, M. J. Pascual, A. Caballero, J. J. Velázquez, J. Mosa, Y. Castro, and A. Durán, "Crystallization mechanism in sol-gel oxyfluoride glass-ceramics," J. Non-Cryst. Solids **501**, 145–152 (2018).
41. M.E. Cruz, J. Li, G. Gorni, A. Durán, G.C. Mather, R. Balda, J. Fernández, and Y. Castro, "Nd3+ doped SiO2-KLaF4 oxyfluoride glass-ceramics prepared by sol-gel.pdf, (2021).
42. D. Chen, Y. Yu, P. Huang, and Y. Wang, "Nanocrystallization of lanthanide trifluoride in an aluminosilicate glass matrix: Dimorphism and rare earth partition," CrystEngComm **11**(8), 1686–1690 (2009).
43. J. J. Velázquez, R. Balda, J. Fernández, G. Gorni, G. C. Mather, L. Pascual, A. Durán, and M. J. Pascual, "Transparent glass-ceramics of sodium lutetium fluoride co-doped with erbium and ytterbium," J. Non-Cryst. Solids **501**, 136–144 (2018).
44. Y. Gao, Y. Hu, D. Zhou, and J. Qiu, "Effect of crystalline fraction on upconversion luminescence in Er^{3+}/Yb^{3+} Co-doped $NaYF_4$ oxyfluoride glass-ceramics," J. Eur. Ceram. Soc. **37**(2), 763–770 (2017).
45. J. J. Velázquez, R. Balda, J. Fernández, G. Gorni, M. Sedano, A. Durán, D. Galusek, and M. J. Pascual, "Structural and optical properties in Tm^{3+}/Tm^{3+}–Yb^{3+} doped $NaLuF_4$ glass-ceramics," Int. J. Appl. Glass Sci. **12**(4), 485–496 (2021).
46. J. J. Velázquez, R. Balda, J. Fernández, G. Gorni, L. Pascual, G. Chen, M. Sundararajan, A. Durán, and M. J. Pascual, "Transparent oxyfluoride glass-ceramics with $NaGdF_4$ nanocrystals doped with Pr^{3+} and Pr^{3+}-Yb^{3+}," J. Lumin. **193**, 61–69 (2018).
47. A. A. Cabral, R. Balda, J. Fernández, G. Gorni, J. J. Velázquez, L. Pascual, A. Durán, and M. J. Pascual, "Phase evolution of $KLaF_4$ nanocrystals and their effects on the photoluminescence of Nd^{3+} doped transparent oxyfluoride glass-ceramics," CrystEngComm **20**(38), 5760–5771 (2018).
48. G. Gorni, J. J. Velázquez, G. C. Mather, A. Durán, G. Chen, M. Sundararajan, R. Balda, J. Fernández, and M. J. Pascual, "Selective excitation in transparent oxyfluoride glass-ceramics doped with Nd^{3+}," J. Eur. Ceram. Soc. **37**(4), 1695–1706 (2017).
49. A. Herrmann, M. Tylkowski, C. Bocker, and C. Rüssel, "Cubic and hexagonal $NaGdF_4$ crystals precipitated from an aluminosilicate glass: Preparation and luminescence properties," Chem. Mater. **25**(14), 2878–2884 (2013).
50. G. Gorni, R. Balda, J. Fernández, L. Pascual, A. Durán, and M. J. Pascual, "Effect of the heat treatment on the spectroscopic properties of Er^{3+} -Yb^{3+} -doped transparent oxyfluoride nano-glass-ceramics," J. Lumin. **193**, 51–60 (2018).
51. L. Fu, "Spark plasma sintered ZrO2-SiO2 glass ceramics and Si3N4 bioceramics Spark plasma sintered ZrO2 -SiO2 glass ceramics and Si3N4 bioceramics," Doctoral thesis, Uppsala University, 2018, (2018).
52. M. Hubert, G. Delaizir, J. Monnier, C. Godart, H.-L. Ma, X.-H. Zhang, and L. Calvez, "An innovative approach to develop highly performant chalcogenide glasses and glass-ceramics transparent in the infrared range," Opt. Express **19**(23), 23513 (2011).
53. Q. Z. Chen, I. D. Thompson, and A. R. Boccaccini, "45S5 Bioglass®-derived glass-ceramic scaffolds for bone tissue engineering," Biomaterials **27**(11), 2414–2425 (2006).
54. S. Cui, C. Boussard-Plédel, L. Calvez, F. Rojas, K. Chen, H. Ning, M. J. Reece, T. Guizouarn, and B. Bureau, "Comprehensive study of tellurium based glass ceramics for thermoelectric application," Adv. Appl. Ceram. **114**(sup1), S42–S47 (2015).
55. S. Kim, B. Kim, and H. Kim, "Optical properties of densified phosphor-in-glass LED encapsulants by spark plasma sintering," Opt. Mater. Express **7**(12), 4304 (2017).
56. B. Xue, L. Calvez, V. Nazabal, X.H. Zhang, G. Delaizir, J. Monnier, G. Martinelli, and Y. Quiquempois, "Mechanical milling and SPS used to obtain GeS_2-βGeS_2 infrared glass-ceramic," J. Non-Cryst. Solids **377**, 240–244 (2013).
57. S. López-Esteban, J. F. Bartolomé, L. A. Díaz, L. Esteban-Tejeda, C. Prado, R. López-Piriz, R. Torrecillas, and J. S. Moya, "Mechanical performance of a biocompatible biocide soda-lime glass-ceramic," J. Mech. Behav. Biomed. Mater. **34**, 302–312 (2014).
58. V. Paygin, E. Dvilis, S. Stepanov, O. Khasanov, D. Valiev, T. Alishin, M. Ferrari, A. Chiasera, V. Mali, and A. Anisimov, "Manufacturing optically transparent thick zirconia ceramics by spark plasma sintering with the use of collector pressing," Appl. Sci. **11**(3), 1304 (2021).
59. M. Tokita, "Spark Plasma Sintering (SPS) Method, Systems, and Applications, Second Edi, Elsevier Inc., 2013. doi:10.1016/B978-0-12-385469-8.00060-5.
60. S. Tanabe, H. Hayashi, T. Hanada, and N. Onodera, "Fluorescence properties of Er^{3+} ions in glass ceramics containing LaF_3 nanocrystals," Opt. Mater. (Amsterdam, Neth.) **19**(3), 343–349 (2002).

Optical Materials EXPRESS

61. Y. Xu, X. Zhang, S. Dai, B. Fan, H. Ma, J. L. Adam, J. Ren, and G. Chen, "Efficient near-infrared down-conversion in Pr^{3+}-Yb^{3+} codoped glasses and glass ceramics containing LaF_3 nanocrystals," J. Phys. Chem. C **115**(26), 13056–13062 (2011).
62. D. Chen, Y. Wang, Y. Yu, and E. Ma, "Influence of Yb^{3+} content on microstructure and fluorescence of oxyfluoride glass ceramics containing LaF_3 nano-crystals," Mater. Chem. Phys. **101**(2-3), 464–469 (2007).
63. G. Gorni, A. Cosci, S. Pelli, L. Pascual, A. Durán, and M. J. Pascual, "Transparent oxyfluoride nano-glass ceramics doped with Pr^{3+} and Pr^{3+}-Yb^{3+} for NIR emission," Front. Mater. 3, (2017).doi:10.3389/fmats.2016.00058.
64. G. Gorni, R. Balda, J. Fernández, I. Iparraguirre, J. J. Velázquez, Y. Castro, L. Pascual, G. Chen, M. Sundararajan, M. J. Pascual, and A. Durán, "Oxyfluoride glass-ceramic fibers doped with Nd^{3+}: Structural and optical characterization," CrystEngComm **19**(44), 6620–6629 (2017).
65. Y. Yu, D. Chen, Y. Wang, W. Luo, Y. Zheng, Y. Cheng, and L. Zhou, "Structural evolution and its influence on luminescence of SiO_2-SrF_2–ErF_3 glass ceramics prepared by sol-gel method," Mater. Chem. Phys. **100**(2-3), 241–245 (2006).
66. M. Tada, S. Fujihara, and T. Kimura, "Sol-gel processing and characterization of alkaline earth and rare-earth fluoride thin films," J. Mater. Res. **14**(4), 1610–1616 (1999).
67. M. E. Cruz, A. Durán, R. Balda, J. Fernández, G. C. Mather, and Y. Castro, "A new sol–gel route towards Nd^{3+} -doped SiO_2 –LaF_3 glass-ceramics for photonic applications," Mater. Adv. **1**(9), 3589–3596 (2020).
68. G. Gorni, R. Balda, J. Fernández, J. J. Velázquez, L. Pascual, J. Mosa, A. Durán, and Y. Castro, "80SiO_2 -20LaF_3 oxyfluoride glass ceramic coatings doped with Nd^{3+} for optical applications," Int. J. Appl. Glass Sci. **9**(2), 208–217 (2018).
69. J. Q. Hong, L. H. Zhang, P. X. Zhang, Y. Q. Wang, and Y. Hang, "Growth, optical characterization and evaluation of laser properties of Nd:LaF_3 crystal," J. Alloys Compd. **646**, 706–709 (2015).
70. Y. Yu, D. Chen, E. Ma, Y. Wang, and Z. Hu, "Spectroscopic properties of Nd^{3+} doped transparent oxyfluoride glass ceramics," Spectrochim. Acta, Part A **67**(3-4), 709–713 (2007).
71. M. Abril, J. Méndez-Ramos, I. R. Martín, U. R. Rodríguez-Mendoza, V. Lavín, A. Delgado-Torres, V. D. Rodríguez, P. Núñez, and A. D. Lozano-Gorrín, "Optical properties of Nd^{3+} ions in oxyfluoride glasses and glass ceramics comparing different preparation methods," J. Appl. Phys. **95**(10), 5271–5279 (2004).
72. R.K. Sharma and P. Ghosh, "Lanthanide-Doped Luminescent Nanophosphors via Ionic Liquids," Front. Chem. **9**, 1–26 (2021).
73. W. Yang, Y. Wang, A. Etogo, J. Ning, Y. Xie, and Y. Hu, "Carbon nanocoating: An effective nanoreactor towards well-defined carbon-coated GaN hollow nanospindles," Nanoscale **6**(6), 3051–3054 (2014).
74. C. P. Groen and A. Oskam, "Theoretical Study of Mixed MLaX 4 (M) Na, K, Cs; X) F, Cl, Br, I) Rare Earth / Alkali Metal Halide Complexes," 42, 851–858 (2003).
75. A. De Pablos-Martín, D. Ristic, A. Durán, M. Ferrari, and M. J. Pascual, "Crystallization and optical properties of Tm^{3+}/Yb^{3+}-co-doped $KLaF_4$ glass-ceramics," CrystEngComm **19**(6), 967–974 (2017).
76. J.R. Vázquez de Aldana, C. Romero, J. Fernandez, G. Gorni, M.J. Pascual, A. Duran, and R. Balda, "Femtosecond laser direct inscription of 3D photonic devices in Er/Yb-doped oxyfluoride nano-glass ceramics," Opt. Mater. Express **10**(10), 2695 (2020).
77. A. S. Kuznetsov, V. K. Tikhomirov, M. V. Shestakov, and V. V. Moshchalkov, "Ag nanocluster functionalized glasses for efficient photonic conversion in light sources, solar cells and flexible screen monitors," Nanoscale **5**(21), 10065–10075 (2013).
78. A. Simo, J. Polte, N. Pfänder, U. Vainio, F. Emmerling, and K. Rademann, "Formation mechanism of silver nanoparticles stabilized in glassy matrices," J. Am. Chem. Soc. **134**(45), 18824–18833 (2012).
79. I. Díez and R.H.A. Ras, "Fluorescent silver nanoclusters," Nanoscale **3**(5), 1963–1970 (2011)..
80. H. Lin, D. Chen, Y. Yu, R. Zhang, and Y. Wang, "Molecular-like Ag clusters sensitized near-infrared down-conversion luminescence in oxyfluoride glasses for broadband spectral modification," Appl. Phys. Lett. **103**(9), 091902 (2013)..
81. J. Ueda, S. Tanabe, and A. Ishida, "Surface plasmon excited infrared-to-visible upconversion in Er^{3+}-doped transparent glass ceramics," J. Non-Cryst. Solids **355**(37-42), 1912–1915 (2009).
82. Q. Liu, Y. Tian, W. Tang, X. Jing, J. Zhang, and S. Xu, "Comprehensive studies of the Ag^{+} effect on borosilicate glass ceramics containing Ag nanoparticles and Er-doped hexagonal $NaYF_4$ nanocrystals: Morphology, structure, and 2.7 μm emission," Nanophotonics **7**(5), 913–923 (2018).
83. J. Zhao, X. Zheng, E. P. Schartner, P. Ionescu, R. Zhang, T. L. Nguyen, D. Jin, and H. Ebendorff-Heidepriem, "Upconversion Nanocrystal-Doped Glass: A New Paradigm for Photonic Materials," Adv. Opt. Mater. **4**(10), 1507–1517 (2016).
84. N. Ojha, M. Tuomisto, M. Lastusaari, and L. Petit, "Upconversion from fluorophosphate glasses prepared with NaYF4:Er^{3+},Yb^{3+} nanocrystals," RSC Adv. **8**(34), 19226–19236 (2018).